Electronic structure of the InAs-GaSb superlattice studied by the renormalization method

G. Grosso
Dipartimento di Fisica, Università degli Studi di Pisa, Centro Interuniversitario di Struttura della Materia (CISM), and Gruppo Nazionale di Struttura della Materia (GNSM), piazza Torricelli 2, I-56100 Pisa, Italy

S. Moroni
Dipartimento di Fisica "Allasandro Volta," Università degli Studi di Pavia, via A. Bassi 6, I-27100 Pavia, Italy

G. Pastori Parravicini
Dipartimento di Fisica, Università degli Studi di Pisa, Centro Interuniversitario di Struttura della Materia (CISM), and Gruppo Nazionale di Struttura della Materia (GNSM), piazza Torricelli 2, I-56100 Pisa, Italy
(Received 1 June 1989)

The electronic band structure of the InAs-GaSb superlattice is studied within the localized-orbital framework by the renormalization method. The tight-binding Hamiltonian includes spin-orbit coupling and an accurate description of the composing crystals near relevant band edges. The tight-binding renormalization-group method is described in detail, and is shown to be conceptually simple and operatively efficient. The superlattice band structure is calculated for several unit-cell widths, and the semiconductor-semimetal transition is analyzed. A negative indirect band gap appears for long-period superlattices; its origin and the effects of band anisotropy and spin-orbit splitting are discussed.

I. INTRODUCTION

The InAs-GaSb superlattice[1,2] has very interesting electronic properties because the relatively large valence-band offset makes it possible to produce a coexistence of spatially separated electron and hole two-dimensional gases,[3] and to tailor the optical gap over a wide range.[4] Although some calculations propose a staggered heterojunction,[5,6] accepted values of the valence-band offset place the bottom of the InAs conduction band lower in energy than the top of the GaSb valence band,[4,7,8] in the so-called "broken gap" configuration.

It was soon recognized that such an unusual lineup opens the possibility for a semiconductor-to-semimetal transition[9] with increasing superlattice period. The transition is experimentally well established by Hall measurements and Shubnikov–de Haas oscillations[10] and by far infrared magnetoabsorption:[11] it takes place at a critical width of the InAs slab of about 100 Å, the GaSb thickness having a minor role. This was predicted within simplified tight-binding model,[9] and confirmed by $\mathbf{k}\cdot\mathbf{p}$ calculations.[12,13] These works exploit a simple quantum size effect in the motion along the superlattice axis: as the wells thickness increases, the lowest superlattice electronlike band approaches the bottom of the InAs conduction band, and eventually it passes below the highest superlattice holelike band, which in turn is raising toward the top of GaSb valence band.

In order to assess the true semimetallic character of the superlattice, however, a detailed analysis of the three-dimensional band structure is needed.[14] The large size of the unit cell prevents direct use of the traditional methods employed in bulk band-structure calculations: for instance, *ab initio* self-consistent calculations performed in the pseudopotential framework are restricted to thin or ultrathin superlattices,[6] and also a simple tight-binding scheme, followed by direct diagonalization, can cope just with medium-size supercells.[15] Also the empirical-pseudopotential approach on folded band structure,[16] though recently applied also to large-period superlattices,[17] seems to require a considerable computational effort. The study of the three-dimensional band structure in the long-period regime was thus performed by a Hartree self-consistent calculation within the envelope-function approximation, leading to the conclusion that the semimetallic behavior is due to extrinsic effects.[14]

In this paper we consider a microscopic description of the InAs-GaSb superlattice Hamiltonian in terms of localized orbitals, and we show that it is possible to obtain the electronic structure, without restrictions on the supercell size, by means of the renormalization method.[18] We find that the interplay of band anisotropy and spin-orbit splitting has important effects on the superlattice band structure, leading to a significant negative indirect band gap and hence to an intrinsic semimetal behavior for long-period superlattices.

In Sec. II, we give a brief overview of the techniques in current use for the study of the large-period superlattice problem, namely the envelope-function approximation[12–14] and the tight-binding complex-$\mathbf{k}$ method[19] (a

 ©1989 The American Physical Society

closely related approach is provided by the transfer matrix,[20] either in the $\mathbf{k}\cdot\mathbf{p}$ formalism[21] or in the tight-binding Green-function framework[22]); we then discuss the motivations of the renormalization and its main features and advantages. In Sec. III, we describe the parametrization of the Hamiltonian, which has been obtained by modifying a semiempirical sp^3s^* model[23] with nearest-neighbor interactions in such a way to include the spin-orbit coupling[24] and to reproduce correct effective masses[25] at the Brillouin-zone center. In Sec. IV we present and discuss our theoretical results together with a comparison with experimental and theoretical work in the literature. Section V contains the conclusions.

II. METHODS OF CALCULATION FOR LONG-PERIOD SUPERLATTICES: THE RENORMALIZATION APPROACH

The study of the semiconductor-semimetal transition in the InAs-GaSb superlattice poses a rather demanding theoretical problem because of the large size of the unit cell. Before presenting in detail the renormalization method, it is worthwhile to briefly summarize the other theoretical tools devised for this kind of problem, together with an overview of advantages and limitations.

A. The envelope-function approximation

An appealing way to overcome the supercell size problem is provided by the envelope-function approximation. The model starts from a $\mathbf{k}\cdot\mathbf{p}$-type Hamiltonian,[26] which is quadratic in $\mathbf{k}$, and accurately describes a few relevant bands of a given bulk material near the band extrema of interest. The superlattice wave functions are expressed as the product of a cell-periodic part (rapidly varying in space) and a multicomponent envelope function, which is smooth on the atomic scale. Then the wave-vector component along the superlattice axis, say k_z, is replaced by the differential operator $-i\,d/dz$; this produces a set of Schrödinger-type differential equations for the envelope function, where the potential has the periodicity of the superlattice, and computational labor is independent of the supercell size. Band anisotropy[27] and spin-orbit interactions[28] can also be included.

The approximation of separating variations on the atomic length scale from those on the envelope-function scale is a valid one only for slowly varying potentials. Since this is not the case for the superlattice potential near the interfaces, the solutions are found within each composing material in the superlattice unit cell, and matched by suitable boundary conditions which assure continuity of the envelope function and conservation of the current density.

These boundary conditions, however, completely overlook the microscopic description of the interfaces, and are justified only when the constituent materials have similar band structure. Moreover, the model Hamiltonian works properly in an energy range which is often smaller than the actual region of interest. Within these limitations, the envelope-function approximation, whenever applicable, gives a reasonable picture of the basic properties of superlattices; at present, considerable interest is drawn by its ability to include in a simple way the effects of magnetic fields.[29]

B. The complex-k method

In order to overcome the intrinsic limitations of the envelope-function approximation, the microscopic description of the crystal must be recovered. A most fruitful microscopic scheme is the localized-orbitals formalism, and the problem of the supercell size can be successful met with the theoretical tools of the complex-$\mathbf{k}$ and renormalization methods.

The complex-$\mathbf{k}$ method[19] rests on two main physical ideas. (i) For a fixed energy, if the crystal wave function is assigned on a small number of adjacent atomic planes, the transfer matrix allows the wave function to be calculated on all the other planes, one (or few) at a time; one thus sees that with an energy-dependent basis set the number of basis functions is small. (ii) In a bulklike region, the bulk complex band structure allows the wave function to be known at once in the whole region.

Operatively, the method is devised to find a superlattice state at a time. A wave vector $\mathbf{q}$ parallel to the superlattice planes and a trial energy E are fixed, and all the bulk eigenstates with those $\mathbf{q}$ and E are found for both materials; these states will have, in general, a complex k_z component along the superlattice axis: a nonzero imaginary part of k_z characterizes decaying states. Then an energy-dependent basis set is built. For instance, one may define the superlattice wave function by its (arbitrary) coefficients on an appropriate number of atomic planes, and then propagate it to the whole supercell by using the transfer matrix at the interfaces and knowledge of the bulk states in bulklike regions. Alternatively, one may expand the superlattice wave function in each material into the corresponding bulk states:[19] this procedure doubles the number of basis functions, but avoids the use of the transfer matrix (if the interfaces are abrupt and the flat band approximation is made) and simplifies the evaluation of the Hamiltonian matrix. The Hamiltonian matrix is then expressed in the energy-dependent basis and diagonalized. The eigenvalue closest to the initial trial energy E is then chosen to restart the whole procedure, which is repeated until convergence is achieved.

C. The renormalization method

The methods developed to solve the superlattice Schrödinger equation within a microscopic description scheme start, in general, from the calculation of the bulk band structure of the composing materials. The renormalization method[18,30,31] is unique in that it works in real space directly on the superlattice problem, and provides a manageable description in terms of the standard layer orbitals $\Phi_{l\lambda}(\mathbf{q})$. Here $\mathbf{q}$ indicates the (k_x,k_y) components of the superlattice Bloch vector $\mathbf{k}$, i.e., $\mathbf{k}=(\mathbf{q},k_z)$, z being the growth axis of the superlattice; l labels the layers of the unit cell (atomic planes can always be grouped in layers, in such a way that interlayer interactions are restricted to nearest neighbors); and finally, λ labels the n in-

dependent orbitals on each layer (we assume for simplicity that n is the same for every layer). On the layer orbital basis, for a given $\mathbf{k}$, the Hamiltonian H of a superlattice composed of N_A layers of material A and N_B layers of material B has a block-tridiagonal form with corner elements which take into account the Bloch boundary conditions:

$$H(\mathbf{q},k_z)=\begin{bmatrix} H_1 & C_1 & & & C_N^{\dagger}e^{-ik_z d} \\ C_1^{\dagger} & H_2 & C_2 & & \\ & C_2^{\dagger} & \ddots & \ddots & \\ & & \ddots & H_{N-1} & C_{N-1} \\ C_N e^{ik_z d} & & & C_{N-1}^{\dagger} & H_N \end{bmatrix} . \tag{1}$$

Here $N=N_A+N_B$, and d is the supercell width. H_l and C_l are $n\times n$ matrices which depend on $\mathbf{q}$:

$$[H_l(\mathbf{q})]_{\lambda,\lambda'}=\langle\Phi_{l,\lambda}(\mathbf{q})|H|\Phi_{l,\lambda'}(\mathbf{q})\rangle ,$$
$$[C_l(\mathbf{q})]_{\lambda,\lambda'}=\langle\Phi_{l,\lambda}(\mathbf{q})|H|\Phi_{l+1,\lambda'}(\mathbf{q})\rangle . \tag{2}$$

Notice that the z component of the superlattice Bloch vector appears only in the corners. From now on, the $\mathbf{q}$ dependence will be implicit. The Hamiltonian H of Eq. (1) is also represented in a schematic way in Fig. 1.

The renormalization method is meant to find the Green function $G(E)=1/(E-H)$ on a given layer l, i.e., the $n\times n$ submatrix $G_l(E)$ with elements $\langle\Phi_{l,\lambda}|G(E)|\Phi_{l\lambda'}\rangle$; the trace of $G_l(E)$, whose imaginary part is proportional to the local density of states on layer l, has a simple pole for each energy corresponding to an eigenvalue of H. In fact, because of the overall periodicity, all states are in general extended and have a nonzero

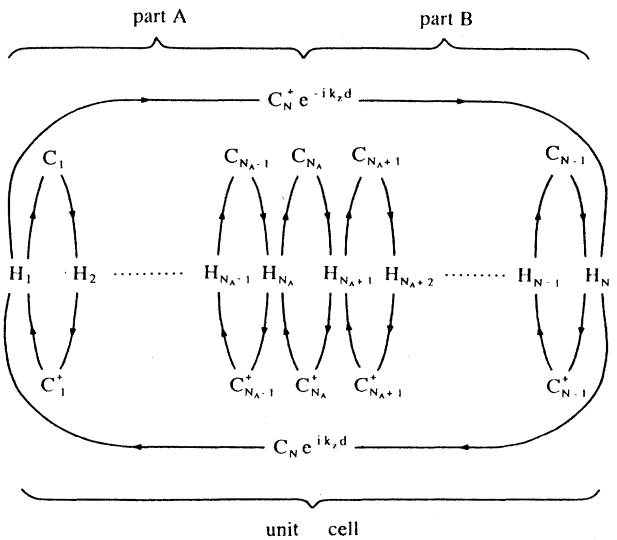

FIG. 1. Schematic representation of the block tridiagonal Hamiltonian (1) as a linear chain: H_m are the on-site interactions, and C_m are the hopping matrices between sites m and $m+1$. Phase factors $e^{\pm ik_z d}$ embody the Bloch boundary conditions.

(though possibly small) contribution on each layer.

The renormalization procedure arrives at the Green function $G_l(E)$, on a given layer l, avoiding the impossible task of direct inversion of the large matrix $E-H$: this purpose is achieved by introducing an $n\times n$ self-energy matrix $\sum_l(E)$ such that

$$G_l(E)=\frac{1}{E-H_l-\sum_l(E)}=\frac{1}{E-H_{\text{eff}}(E)} . \tag{3}$$

The calculation of the energy-dependent self-energy operator is performed via partitioning techniques;[18] it involves only an appropriate use of the Dyson equation. Formal aspects have been discussed elsewhere;[30] we focus here on relevant technical aspects, and in particular, we provide here for the first time a stable algorithm for the calculation of wave functions, and not only of eigenvalues.

The calculation of $H_{\text{eff}}(E)$ is performed by successive decimation of all layers but that of interest. For instance, let layer m be eliminated; a modified, or renormalized, Hamiltonian $H^{(R)}(E)$ is then defined on the remaining layers. In the renormalized Hamiltonian, the matrix elements H_m and C_m are removed, and the following matrix elements are modified:

$$H_{m-1}^{(R)}=H_{m-1}+C_{m-1}\frac{1}{E-H_m}C_{m-1}^{\dagger} ,$$
$$H_{m+1}^{(R)}=H_{m+1}+C_m^{\dagger}\frac{1}{E-H_m}C_m , \tag{4}$$
$$C_{m-1}^{(R)}=C_{m-1}\frac{1}{E-H_m}C_m$$

[it is assumed that possible values of the indices 0 and $N+1$ are replaced by N and 1, respectively; it is also assumed that C_N is multiplied by the same phase factors as in (1)]. Notice that, since the superlattice spectrum is discrete for a given $\mathbf{k}$, we can take E as a real number, so that the renormalized Hamiltonian $H^{(R)}(E)$ is Hermitian; for physical systems with a continuous spectrum, like surfaces and single interfaces,[30–33] a positive imaginary part ε must be added to the energy E, and Eqs. (4) must be generalized to the non-Hermitian case.

Numerical calculation of Eqs. (4) requires only the inversion of the small matrix $E-H_m$ (plus matrix multiplication and addition). The physical meaning of the performed elimination is that the renormalized Hamiltonian and the original one are equivalent for the calculation of the Green function on the remaining layers.

It is easily seen that the block-tridiagonal form of the Hamiltonian is preserved by Eqs. (4), so that the procedure can be iterated. Successive single-layer eliminations are analogous to repeated transfers of the wave function using the transfer matrix; however, the renormalization is numerically stable even after many iterations, while, in general, the transfer-matrix algorithm is not. This circumstance would be of interest in the case of large disrupted (non-bulk-like) regions, for instance if band bending were considered in some extent.

In bulklike regions a substantial improvement of the

efficiency is obtained eliminating simultaneously every other layer. We have implemented a program code which exploits in a simple way this local symmetry, along the following lines. Consider sites 1 through N_A of the ring-shaped linear chain represented by Hamiltonian (1), and suppose that matrices $H_l \equiv H_A$ and $C_l \equiv C_A$ in material A are independent of the layer index l. We allow only H_1 and H_{N_A} to be different from the bulk value H_A (this situation is always met after single-layer eliminations of disrupted interfacial zones, if any). Let us now define N_r as the index of the rightmost preserved layer of part A: at this stage, $N_r = N_A$; it can be assumed that N_r is an odd number [if it is not, layer N_r is removed using Eqs. (4) and the desired situation is recovered without changing the form (1) of the Hamiltonian]. Now all the layers with even index from 2 to $N_r - 1$ are *simultaneously* eliminated by the following simple generalization of Eqs. (4):

$$H_1^{(R)} = H_1 + C_A \frac{1}{E - H_A} C_A^\dagger ,$$
$$H_{N_r}^{(R)} = H_{N_r} + C_A^\dagger \frac{1}{E - H_A} C_A \qquad (5a)$$

for the boundary layers, and

$$H_A^{(R)} = H_A + C_A \frac{1}{E - H_A} C_A^\dagger + C_A^\dagger \frac{1}{E - H_A} C_A ,$$
$$C_A^{(R)} = C_A \frac{1}{E - H_A} C_A \qquad (5b)$$

for the internal odd layers. Again, only the small matrix $E - H_A$ has to be numerically inverted; this time, however, $(N_r - 1)/2$ layers are removed in a single step. Equations (5) can be iterated, possibly after a single layer elimination, to make odd the number of preserved layers in material A. As a result, a small number of renormalizations of the order of $\log_2 N_A$ reduces the whole part A of the supercell to the single layer with $l = 1$.

Treating part B along the same guideway (it is now convenient to define N_l as the leftmost preserved layer in part B), one is left with layers 1 and N. The last step is the calculation of the effective Hamiltonian $H_{\text{eff}}(E)$ by eliminating layer N; finally, the Green function $G_1(E)$ is obtained by Eq. (3).

The described iterative decimation is very efficient: in practice, it is possible to scan the energy range of interest, looking for poles of the Green function. The method presents a remarkable advantage in the calculation of band dispersion along k_z; namely, until layers 1 and N are preserved, all the operations of the renormalization procedure are independent of k_z (i.e., $C_N e^{ik_z d}$ is never involved): it is only the very last step which manipulates k_z-dependent matrix elements, and which has to be repeated, with minor additional labor, as k_z is changed. We can thus obtain as a by-product the k_z-projected superlattice bands.

Another important novelty of the present paper is to provide a stable and efficient algorithm for the study of localization properties of superlattice states. For this purpose, we have devised the following procedures. The first one, which is stable, simply repeats the whole decimation, preserving in turns different layers of interest; however, it would highly desirable not to repeat all of the calculation from the very beginning for each layer. At first sight, a possibility seems to propagate the local Green function (and hence the wave-function amplitude, from the residue at the pole) to successive layers, in close similarity with the transfer-matrix approach. Like the transfer-matrix algorithm, however, this procedure is not numerically stable, so that it can be carried out only for a few tens of layers. Suppose we have eliminated all layers but those with indices m and $m+1$: the Green function can be calculated there, but now we want to find it on layer $m+2$. We indicate by the schemes (a) and (b) in Fig. 2, respectively, the renormalized Hamiltonians in which only layers m and $m+1$, and layers m, $m+1$, and $m+2$, are preserved. All renormalized matrices in (b) are assumed to be known. We can formally pass from the scheme (b) to (a) in Fig. 2, eliminating layer $m+2$ by Eqs. (4); this formal relation can be inverted and solved for the three unknown matrices $\bar{H}_m^{(R)}$, $H_{m+2}^{(R)}$, and $C_{m+2}^{(R)}$, whose expression is:

$$\bar{H}_m^{(R)} = H_m^{(R)} - C_{m+1}^{(R)\dagger} \frac{1}{H_{m+1}^{(R)} - H_{m+1}} C_{m+1}^{(R)} ,$$
$$H_{m+2}^{(R)} = E - C_{m+1}^\dagger \frac{1}{H_{m+1}^{(R)} - H_{m+1}} C_{m+1} , \qquad (6)$$
$$C_{m+2}^{(R)} = C_{m+1}^\dagger \frac{1}{H_{m+1}^{(R)} - H_{m+1}} C_{m+1}^{(R)} .$$

Now layer m is eliminated in (b), again by Eqs. (4): we have thus the possibility of evaluating the Green function on layer $m+2$, and of continuing this procedure to layer $m+3$, and so on.

The above procedure is not numerically stable and it is thus of limited help. However, we have been able to overcome numerical problems with the following algorithm. In order to describe it, we look for the Green function on a couple of adjacent layers at an arbitrary position within the unit supercell, say on layers m and $m+1$. As schematically shown in Fig. 3(a), we divide the unit supercell in part $S_<(m+1)$, which contains all layers with index less than $m+1$, and part $S_>(m)$, which

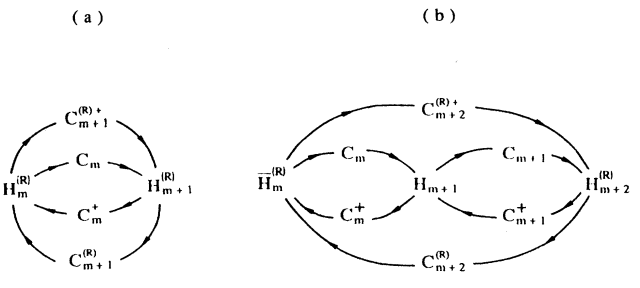

FIG. 2. Schematic representation of the renormalized Hamiltonians acting (a) on layers m and $m+1$ and (b) on layers m, $m+1$, and $m+2$; matrices without the superscript (R) are the same as in the original Hamiltonian (1).

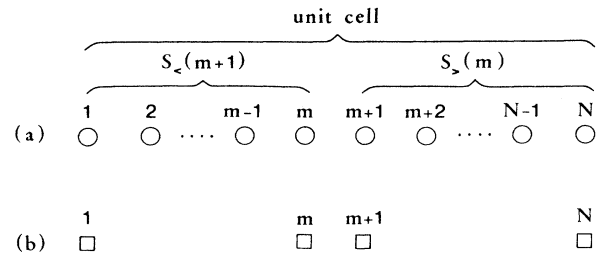

FIG. 3. Partition of the unit-supercell into $S_<(m+1)$ and $S_>(m)$. Circles in (a) indicate the N layers of the supercell; by introducing the renormalized Hamiltonians $H_<^{(R)}(m+1)$ and $H_>^{(R)}(m)$, the system is reduced to layers 1, m, $m+1$, and N indicated by squares in (b).

contains all layers with index larger than m. We now manipulate part $S_<(m+1)$ by single-layer elimination [Eqs. (4)] of layers $2,3,\ldots,m-1$, thus obtaining the renormalized Hamiltonian $H_<^{(R)}(m+1)$ which is defined only on layers 1 and m. Similarly, in part $S_>(m)$ we successively remove layers $N-1,N-2,\ldots,m+2$, and calculate the renormalized Hamiltonian $H_>^{(R)}(m)$ acting on layers $m+1$ and N. At this stage the whole unit supercell is reduced to layers 1, m, $m+1$, and N [Fig. 3(b)], and it is described by a renormalized Hamiltonian expressed in terms of $H_<^{(R)}(m+1), H_>^{(R)}(m)$ and the interactions among $S_<(m+1)$ and $S_>(m)$, namely C_m and $C_N e^{ik_z d}$ (see Fig. 1). Four renormalizations are still required to find the Green function on layers m and $m+1$.

The motivation of obtaining $H_<^{(R)}(m+1)$ and $H_>^{(R)}(m)$ by successive elimination of single layers is that if we also need the Green function on layers $m+2$ and $m+3$, we do not have to restart the procedure from the beginning. In fact, $H_<^{(R)}(m+3)$ is readily obtained from $H_<^{(R)}(m+1)$ by simply removing layers m and $m+1$ in part $S_<(m+3)$; furthermore, $H_>^{(R)}(m+2)$ is already known, if we store the partial results of the already performed successive elimination of layers $N-1,N-2,\ldots,m+2$ in part $S_>(m)$, i.e., the renormalized Hamiltonians $H_>^{(R)}(N-2), H_>^{(R)}(N-3),\ldots,H_>^{(R)}(m)$. As a result, the calculation of the Green function at every layer of the unit supercell requires a total of $4N$ renormalizations.

The renormalization method is very satisfactory from a conceptual point of view: it unifies the treatment of different situations such as interfaces and disrupted and bulklike zones in the simple formalism summarized in Eqs. (4) and their generalization (5); each step of the iterative elimination procedure has a transparent physical meaning in terms of a renormalized Hamiltonian acting on the preserved layers. In the new implementation along the lines here described, the method is extended to the evaluation of the wave-function amplitude and to the very easy determination of the k_z-projected band structure.

III. THE TIGHT-BINDING MODEL HAMILTONIAN

Semiempirical tight-binding schemes have been widely used to study a variety of semiconductor layered structures with moderate computational requirements. The main bulk features are reproduced by judicious adjustment of the independent matrix elements of the model; relevant situations in semiconductor microstructures, such as relaxation, alloying, strain, and interface dipoles are easily included in the model, giving correct physical trends. In a number of cases, tight-binding calculations have provided a valuable predictive guide to the main physical properties of the problem at hand, which have been confirmed by more realistic *ab initio* calculations.

Following a widely used parametrization scheme,[23] we describe the bulk InAs and GaSb crystals by a nearest-neighbor interaction tight-binding model with sp^3s^* orbitals per atom. However, we have several different requirements on the parametrization; it must include spin-orbit coupling and give an accurate account of the energy bands and effective masses near the fundamental gap. Notice that with the sp^3s^* spin-orbit model the matrices H_l and C_l defined in Eq. (2) are of order 10×10 for the (001) grown superlattices.

In Ref. 23, the independent matrix elements are fitted to the known bulk band energies' differences at the symmetry points Γ and X, neglecting spin-orbit coupling. In a superlattice, on the contrary, one is usually interested in energies near the fundamental gap of the constituent materials, and it is thus important to give an accurate description of the bulk band dispersion in that region, including the spin-orbit coupling. Thus we have to find an alternative parametrization procedure, suitable to our purpose.

For this purpose it seemed natural to start from the $\mathbf{k}\cdot\mathbf{p}$ model.[26] The $\mathbf{k}\cdot\mathbf{p}$ method features are as follows: use of the cell-periodic part of the bulk Bloch functions at a given $\mathbf{k}_0$ as a basis set; quadratic expansion in $\mathbf{k}-\mathbf{k}_0$; and restriction to a few bands in a selected energy range, other bands being possibly considered by second-order perturbation. The same procedure can be explicitly carried out for a tight-binding Hamiltonian at the Γ point. Analytic relations between tight-binding and $\mathbf{k}\cdot\mathbf{p}$ quantities are thus obtained. In order to change the original parametrization of Ref. 23 as little as possible, we exploit only two of these relations, modifying the tight-binding independent matrix elements in such a way to reproduce the values of the Luttinger parameters γ_1 and γ_2 given by Lawaetz[25] (Luttinger parameters γ_1, γ_2, and γ_3 describe the dispersion of heavy- and light-hole bands in the $\mathbf{k}\cdot\mathbf{p}$ formalism). The modified tight-binding parameters, listed in Table I, produce also values of γ_3 and m_c, the conduction-band effective mass, in good agreement, within typical uncertainties of these parameters, with Lawaetz's ones.[25]

We describe the superlattice Hamiltonian in the flat band approximation: diagonal terms in GaSb are shifted by the valence-band offset E_{VBO}. This very important quantity is taken as an empirical input parameter. In order to compare our results with Ref. 14, we set $E_{\mathrm{VBO}}=0.57$ eV. The resulting bulk band structures of

TABLE I. Tight-binding parameters for InAs and GaSb, in eV. Notations are as in Refs. 23 and 24. These parameters place the top of the valence band at 0.0 eV both in InAs and GaSb. The Luttinger parameters γ_1, γ_2 and γ_3 and the conduction-band effective mass m_c, calculated from our tight-binding model, are also listed. For comparison we report in parentheses the values taken from Ref. 25.

	InAs	GaSb
$E(s,a)$	−9.5381	−7.3207
$E(p,a)$	0.7715	0.5949
$E(s^*,a)$	7.4099	6.6354
$E(s,c)$	−2.7219	−3.8993
$E(p,c)$	3.5817	2.6541
$E(s^*,c)$	6.7401	5.9846
$V(s,s)$	−5.6052	−6.1567
$V(x,x)$	1.8398	1.5789
$V(x,y)$	4.9419	4.8261
$V(s_a,p_c)$	3.7914	6.1569
$V(s_c,p_a)$	6.7934	5.7937
$V(s_a^*,p_c)$	3.3744	4.9895
$V(s_c^*,p_a)$	3.9097	4.2180
Δ_a	0.421	0.973
Δ_c	0.392	0.714
γ_1	19.67(19.67)	11.8(11.8)
γ_2	8.37(8.37)	4.03(4.03)
γ_3	9.13(9.29)	5.04(5.26)
m_c	0.024(0.023)	0.050(0.045)

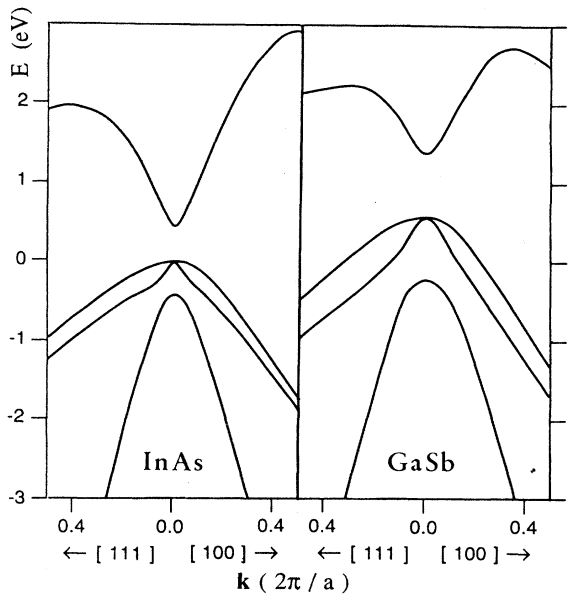

FIG. 4. Bulk band structures of InAs and GaSb near the fundamental gap, calculated by the tight-binding parameters displayed in Table I. The zero of the energy is taken at the top of the InAs valence band.

InAs and GaSb near the fundamental gap are displayed in Fig. 4; the energy zero is taken at the top of InAs valence band.

The interaction parameters across the interfaces are taken equal to the bulk values[23] for InSb and GaAs, respectively; this choice has a noticeable effect on some of the results to be presented, showing the importance of the microscopic features of the interfaces even for large-period superlattices. A related problem is raised by the values of the number of layers N_A and N_B [in InAs-GaSb (001) superlattices, with only nearest-neighbor interactions, a layer is formed by a single atomic plane of either anions or cations]. If N_A and N_B are even numbers, both interfaces between In and Sb atoms and between Ga and As are alternatively present. If N_A and N_B are odd, the same pair of atoms, either In and Sb or Ga and As, occur at each interface. As expected this "microscopic" difference in the interfaces affects the electronic structure, mainly (but not only) for small-period superlattices. We do not pursue further this question, and present only results obtained with N_A and N_B even.

IV. RESULTS FOR THE InAs-GaSb (001) SUPERLATTICE

In this section we present our results, with the aim to clarify the physical mechanisms which drive the onset of the semimetallic behavior. Although some quantitative features of the reported band structures are to be taken with caution, because they are very sensitive to the value of the valence-band offset E_{VBO}, the mechanisms of indirect gap formation are to a large extent independent of it. The choice of interaction parameters across the interfaces can have small, but not negligible, effects on the superlattice band structure: if we replace values reported in Table I by a mean from InAs and GaSb parameters, we have changes in the superlattice band dispersion of the order of the meV. This is rather surprising, in view of the large number of layers in the unit supercell. The importance of the microscopic structure of the interfaces is supported by the wave-function amplitude, which often shows a strong asymmetry with respect to the center of the slab of (for instance) GaSb, as a consequence of the difference between the two interfaces; this asymmetry of course disappears for superlattices with odd values of N_A and N_B.

Figure 5 illustrates the evolution of the $N_A = N_B$ superlattice band structure versus the supercell width. Here the wave-vector components $\mathbf{q}$ parallel to the superlattice planes are zero, and the dispersion along z is projected. Mixing and anticrossing behavior occur; anyhow, far from mixing regions, it is possible to retain the overall distinction between the almost dispersionless heavy-hole bands and the light-particle ones, with noticeable bandwidth even for large-period superlattices. As the supercell size increases, holelike states raise toward the top of the GaSb valence band, and the electronlike states approach the bottom of the InAs conduction band. The lowest electronlike band $E1$ passes below the highest heavy-hole band HH1 for $N_A = 66$, in close agreement with the experimental value of about 100 Å for the semiconductor-semimetal transition.

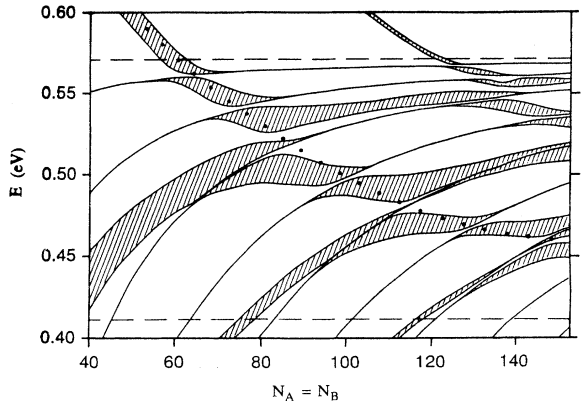

FIG. 5. Evolution of the superlattice band structure for $\mathbf{q}=(0,0)$ versus the unit-supercell size; the dispersion along k_z is projected. Dashed lines indicate the top of the GaSb valence band and the bottom of the InAs conduction band; the dotted line is simply a guide for the eye to the evolution of the lowest InAs electronlike subband $E1$.

This critical width is very sensitive to the valence-band offset. This is expected on the basis of simple quantum size considerations of light and heavy particles; near the top of the GaSb bulk valence band, and for $\mathbf{q}=(0,0)$, the dispersionless heavy-hole bands behave like discrete levels of the one-dimensional motion in a quantum well with infinite potential barriers; even changing the valence-band offset to 0.52 eV,[19] their position with respect to the "well top" (the GaSb valence-band maximum) does not change by more than 1 meV. On the other hand, the light electrons in $E1$ are not near the "well bottom," which is now the InAs conduction-band minimum; they can be confined by lower barriers only if the superlattice period is increased. As a result, for instance, with $E_{\mathrm{VBO}}=0.52$ eV the critical width corresponds to $N_A=80$.

The classification of superlattice states in terms of bulklike states of individual composing materials is justified, in this range of energy, by localization properties and orbital character. Some examples are given by the wave-function amplitudes displayed in Fig. 6. The represented states are in a mixing region of HH4 and $E1$. In Fig. 6(a) the heavy-hole component is prevalent: the state is almost completely localized in GaSb, where it has p_x and p_y orbital character and it shows a structure with three nodes, like the fourth energy level of a particle confined in a quantum well. In Fig. 6(b) the state is more electronlike: the wave function is mainly localized in InAs, where s character dominates; however, due to its light mass, the electron can penetrate in GaSb, where it induces a noticeable p_z amplitude which adds to a remainder of the three nodes' heavy-hole contribution. Notice also the asymmetry of the wave-function amplitude with respect to the center of the slab of (for instance) GaSb, and the jumps near the InSb interface; it would be interesting to relate these features to the electronic structure of the interfaces.

The interchange in relative position of bands $E1$ and

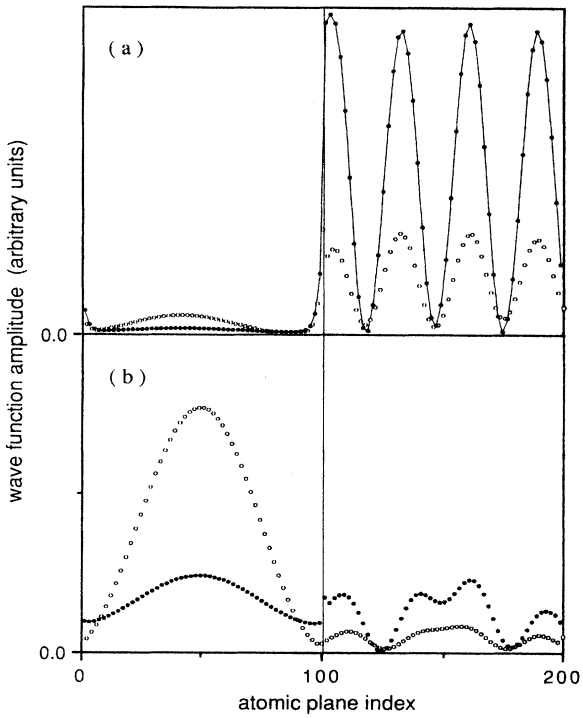

FIG. 6. Wave-function amplitudes for the states at (a) $E=0.4986$ eV, $\mathbf{k}=(0,0,4\pi/Na)$ and (b) $E=0.4860$ eV, $\mathbf{k}=(0,0,4\pi/Na)$ for the superlattice with $N_A=N_B=100$ (for each atomic plane, the plotted quantity is $\sum_\lambda |c_{l\lambda}|^2$, where $c_{l\lambda}$ are the coefficients of the wave-function expansion in terms of the layer orbitals $\Phi_{l\lambda}$). Solid and open circles indicate anions and cations, respectively; planes 1–100 are InAs, 101–200 are GaSb.

HH1 at $\mathbf{q}=(0,0)$ is not a sufficient condition for the onset of the semimetallic regime: a close inspection of the superlattice three-dimensional band structure is needed. Figures 7–9 show the superlattice bands near the Fermi level for $\mathbf{k}$ with components $\mathbf{q}$ along the [100] and [110] directions for different unit-cell thicknesses. Dispersion along k_z is projected: notice that this allows a wealth of information to be synthetically displayed and analyzed. Besides the strong nonparabolicity of the bands and their quasi-two-dimensional behavior for large enough values of $|\mathbf{q}|$, notice the anisotropy with respect to the directions of $\mathbf{q}$ and the lifting of spin-orbit degeneracy present at $\mathbf{q}=(0,0)$: both these effects have a magnitude of several meV, which is relevant on the superlattice-bands energy scale.

For $N_A=N_B=64$ (Fig. 7) it appears that bands $E1$ and HH1 are mixed even at $\mathbf{q}=(0,0)$, where a gap of 2.6 meV opens. For $\mathbf{k}$ off the $\mathbf{z}$ direction, the superlattice conduction band starts moving downward; however, the resulting indirect gap is exceedingly small (of the order of 0.1 meV) and it disappears altogether as the superlattice period is increased. These results qualitatively agree with the conclusions of the envelope-function-approximation calculation of Ref. 14. However, if the superlattice period is further increased, something new happens, and a relevant indirect gap does appear. For $N_A=N_B=100$

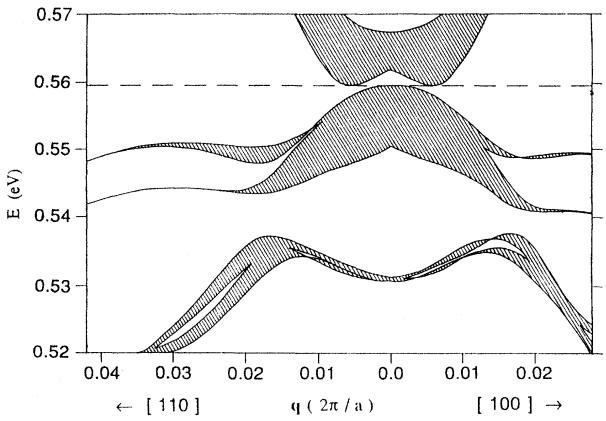

FIG. 7. Band structure of the superlattice with $N_A = N_B = 64$ for **k** off the z direction. Dispersion along k_z is projected. The top of the valence band and the bottom of the conduction band almost coincide; they are indicated by the dashed line. At $\mathbf{q}=(0,0)$, the two upper bands are a mixing from $E1$ and HH1, and the lower one is HH2.

(Fig. 9), its size has reached 3.5 meV, and the **k**-space region where the conduction band lies below the valence-band maximum is rather large.

We now want to briefly comment on the employed flat band approximation. The main effect of the Hartree self-consistent description of the charge transfer from GaSb to InAs was shown[14] to be a raising of superlattice states mainly localized in InAs, and a lowering of those localized in GaSb; such an effect is not expected to substantially modify the balance of spin-orbit and anisotropy effects and anticrossing behavior that we are discussing. As for the charge transfer from superlattice valence and conduction bands due to the presence of the negative indirect gap, we note that near the Fermi level [at least in simple situations such as that of Fig. 6(a)] both these bands are mainly GaSb holelike states, with some InAs electronlike admixture in the small mixing region; as a result, we expect that this effect causes no relevant charge

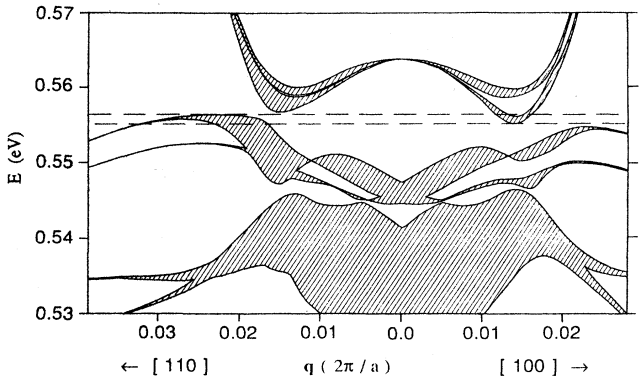

FIG. 8. Band structure of the superlattice with $N_A = N_B = 80$ for **k** off the z direction. Dispersion along k_z is projected. The top of the valence band and the bottom of the conduction band are indicated by dashed lines. At $\mathbf{q}=(0,0)$, the upper band is HH1, and the lower ones are a mixing from HH2 and $E1$.

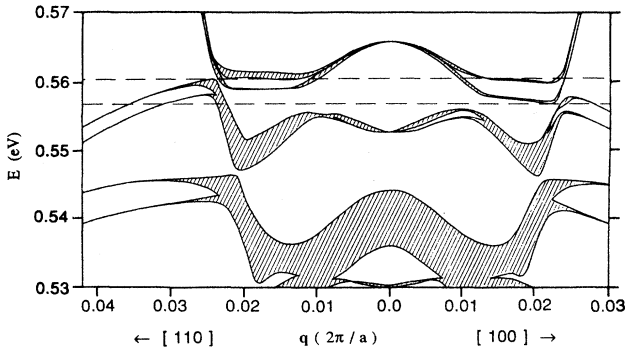

FIG. 9. Band structure of the superlattice with $N_A = N_B = 100$ for **k** off the z direction. Dispersion along k_z is projected. The top of the valence band and the bottom of the conduction band are indicated by dashed lines. At $\mathbf{q}=(0,0)$, bands HH1, HH2, LH1, and HH3 are displayed. The parabola which represents the upward-dispersing electronlike band $E1$ can be identified (though its bottom is off the scale).

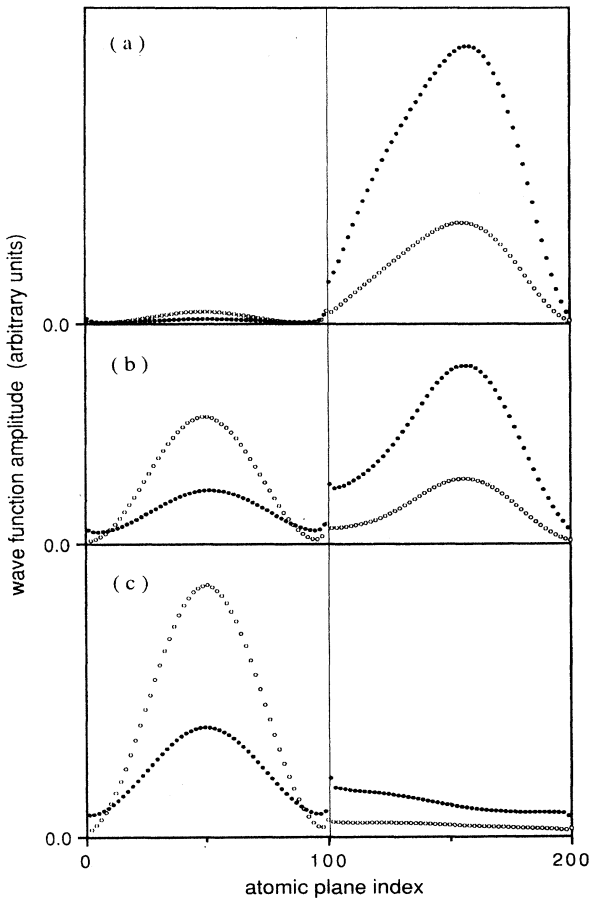

FIG. 10. Wave-function amplitude for the states at (a) $E = 0.5570$ eV, $\mathbf{k}=(0.022,0,0)2\pi/a$; (b) $E = 0.5577$ eV, $\mathbf{k}=(0.024,0,0)2\pi/a$; (c) $E = 0.5641$ eV, $\mathbf{k}=(0.026,0,0)2\pi/a$ for the superlattice with $N_A = N_B = 100$. Solid and open circles indicate anions and cations, respectively. These states are on the lower component of the spin-orbit-split superlattice conduction band (see Fig. 9). (a) is completely holelike, (b) is of intermediate character, and (c) is electronlike.

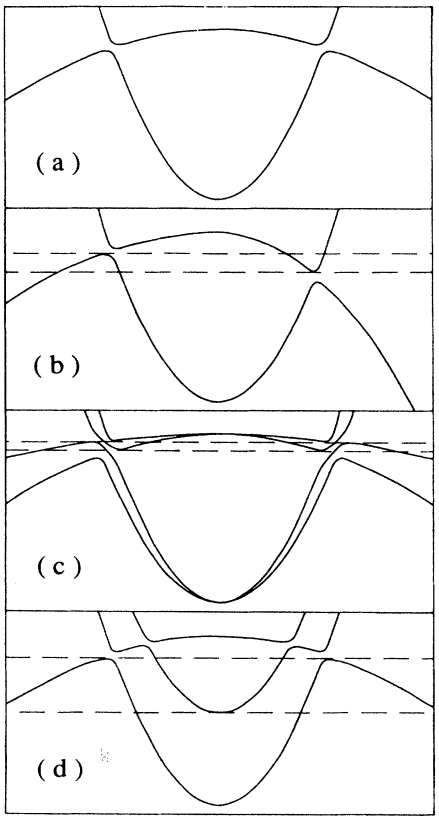

FIG. 11. (a) Schematic representation of the dispersion of a holelike and an electronlike band: though at $k=0$ the electronlike band is lower in energy, the formation of a negative gap is prevented by the anticrossing behavior. A negative indirect gap can be obtained by (b) holelike band anisotropy, (c) spin-orbit splitting, and (d) mixing of several bands. In (b), (c), and (d) dashed lines indicate the top of the "valence" band and the bottom of the "conduction" band.

transfer in space.

These considerations indicate that, even in the presence of band-bending effects, the intrinsic semimetallic character can be explained by the following mechanisms. In Fig. 9, the parabola (slightly spread by k_z dispersion) which represents the InAs electronlike band $E1$ can be recognized. When $E1$ approaches the GaSb heavy-hole-like band HH1, the region of mixing is very small, and the bands soon recover their original character and dispersion (this behavior can be quantitatively analyzed in terms of localization properties and the orbital character of superlattice states; for instance, Fig. 10 shows that the superlattice conduction band is heavy-hole-like before the mixing region, of intermediate nature where $E1$ and HH1 mix, and electronlike at larger values of q). Then a key role in yielding the negative indirect gap is assumed by the holelike bands' anisotropy and by the spin-orbit splitting in the way schematically represented in Figs. 11(b) and 11(c). For comparison, notice that for $N_A=N_B=64$ (Fig. 7) mixing of $E1$ and HH1 occurs in a wide region near the bottom of the parabola; here q is small, as well as the spin-orbit splitting and the band anisotropy shift, so that the effect of anticrossing behavior prevails, and no indirect gap, or a very tiny one, forms.

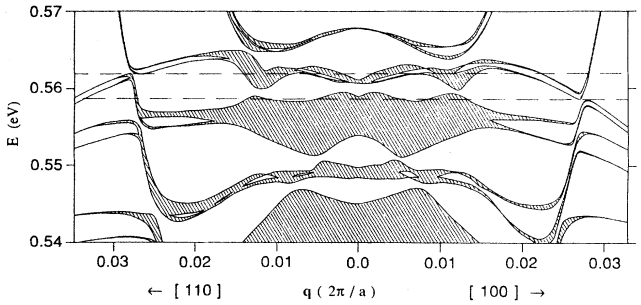

FIG. 12. Band structure of the superlattice with $N_A=N_B=140$ for **k** off the z direction. Dispersion along k_z is projected. The top of the valence band and the bottom of the conduction band are indicated by dashed lines. The negative indirect gap size is given by band anisotropy and spin-orbit splitting; however, notice that in the [110] direction the conduction band has a local minimum, which is lower than the valence-band maximum as a result of the presence of the second electronlike band $E2$ [see also Fig. 11(c)].

The reported results are an illustration of a general trend verified also with the different parametrization of the Hamiltonian of Ref. 19 over a wide range of superlattice periods. However, for even larger superlattice periods the situation can be more complicated. For $N_A=N_B=140$ (Fig. 12), besides the already discussed effects, we can observe the onset of a different mechanism capable of giving semimetallic character: the superlattice valence-band top is for **q** in the [110] direction, where $E2$ and HH1 mix; for **q** in the same direction, we find a local minimum of the conduction band which provides a negative indirect gap independent of band anisotropy. This mechanism can be explained, in terms of crossing among several bands, in the way schematically indicated in Fig. 11(d).

V. CONCLUSION

We have presented a detailed discussion of the renormalization method for the calculation of superlattice band structure and wave functions; in particular we have provided a stable and efficient procedure not only for the calculation of superlattice eigenvalues, but also for superlattice eigenfunctions. We have studied, within the localized-orbital formalism, the electronic structure of the InAs-GaSb superlattice in the semimetal regime. A relevant negative indirect gap is found, whose origin is interpreted as an effect of band anisotropy and spin-orbit coupling. The results of the present paper for the difficult InAs-GaSb superlattice should stimulate a more widespread application of the renormalization method and its concepts in the study of the physical properties of superlattices and microstructures.

ACKNOWLEDGMENTS

This work has been partially supported by Commissione delle Comunità Europee, under Contract No. ST2J-0254-2-I.

[1]G. A. Sai-Halasz, R. Tsu, and L. Esaki, Appl. Phys. Lett. **30**, 651 (1977).
[2]L. Esaki, IEEE J. Quantum Electron. **QE-22**, 1611 (1986).
[3]L. L. Chang, G. A. Sai-Halasz, and L. Esaki, J. Vac. Sci. Technol. **19**, 589 (1981).
[4]G. A. Sai-Halasz, L. L. Chang, J. M. Welter, C. A. Chang, and L. Esaki, Solid State Commun. **27**, 935 (1978).
[5]W. R. Frensley and H. Kroemer, Phys. Rev. B **16**, 2642 (1977).
[6]J. Ihm, P. K. Lam, and M. L. Cohen, Phys. Rev. B **20**, 4120 (1979).
[7]L. L. Chang, in *Semiconductors Superlattices and Heterostructures,* edited by G. Allan, G. Bastard, N. Boccara, M. Lannoo, and M. Voos (Springer-Verlag, Berlin, 1986).
[8]G. J. Gualtieri, G. P. Schwartz, R. G. Nuzzo, R. J. Malik, and J. F. Walker, J. Appl. Phys. **61**, 5337 (1987).
[9]G. A. Sai-Halasz, L. Esaki, and W. A. Harrison, Phys. Rev. B **18**, 2812 (1978).
[10]L. L. Chang, N. J. Kawai, G. A. Sai-Halasz, R. Ludecke, and L. Esaki, Appl. Phys. Lett. **35**, 939 (1979); L. L. Chang, N. J. Kawai, E. E. Mendez, C. A. Chang, and L. Esaki, Appl. Phys. Lett. **38**, 30 (1981).
[11]Y. Guldner, J. P. Vieren, P. Voisin, and M. Voos, Phys. Rev. Lett. **45**, 1719 (1980); J. C. Maan, Y. Guldner, J. P. Vieren, P. Voisin, M. Voos, L. L. Chang, and L. Esaki, Solid State Commun. **39**, 683 (1981).
[12]S. R. White and L. J. Sham, Phys. Rev. Lett. **47**, 879 (1981).
[13]G. Bastard, Phys. Rev. B **24**, 5693 (1981); **25**, 7584 (1982).
[14]M. Altarelli, Phys. Rev. B **28**, 842 (1983).
[15]A. Madukhar, N. V. Dandekhar, and R. N. Nucho, J. Vac. Sci. Technol. **16**, 1507 (1979).
[16]M. A. Gell, K. B. Wong, D. Ninno, and M. Jaros, J. Phys. C **19**, 3821 (1986).
[17]Jian-Bai Xia, Phys. Rev. B **39**, 3310 (1989).
[18]R. D. Graft, G. Pastori Parravicini, and L. Resca, Solid State Commun. **57**, 699 (1986); R. D. Graft, D. J. Lohrmann, G. Pastori Parravicini, and L. Resca, Phys. Rev. B **36**, 4782 (1987).
[19]J. N. Schulman and Yia-Chung Chang, Phys. Rev. B **31**, 2056 (1985).
[20]D. H. Lee and J. D. Joannopoulos, Phys. Rev. B **23**, 4988 (1981); **23**, 4997 (1981).
[21]L. R. Ram-Mohan, K. H. Yoo, and R. L. Aggarwal, Phys. Rev. B **38**, 6151 (1988).
[22]M. C. Muñoz, V. R. Velasco, and F. García-Moliner, Phys. Rev. B **39**, 1786 (1989).
[23]P. Vogl, H. P. Hjalmarson, and J. D. Dow, J. Phys. Chem. Solids **44**, 365 (1983).
[24]D. J. Chadi, Phys. Rev. B **16**, 790 (1977).
[25]P. Lawaetz, Phys. Rev. B **4**, 3460 (1971).
[26]E. O. Kane, in *Semiconductors and Semimetals,* edited by R. K. Willardson and A. C. Beer (Academic, New York, 1966), Vol. 1, p. 75.
[27]G. Platero and M. Altarelli, Phys. Rev. B **36**, 6591 (1987).
[28]D. L. Smith and C. Mailhiot, Phys. Rev. B **33**, 8345 (1986); **33**, 8360 (1986).
[29]A. Fasolino and M. Altarelli, Surf. Sci. **142**, 322 (1984).
[30]P. Giannozzi, G. Grosso, S. Moroni, and G. Pastori Parravicini, Appl. Num. Math. **4**, 273 (1988).
[31]G. Grosso, S. Moroni, and G. Pastori Parravicini, Phys. Scr. **T25**, 316 (1989); P. Giannozzi, G. Grosso, and G. Pastori Parravicini, Riv. Nuovo Cimento (to be published).
[32]F. Guinea, C. Tejedor, F. Flores, and E. Louis, Phys. Rev. B **28**, 4397 (1983).
[33]G. Grosso, S. Moroni, and G. Pastori Parravicini, Phys. Scr. **37**, 930 (1988).